annalen der physik
www.ann-phys.org

Suppression of the Verwey Transition by Charge Trapping

Carolin Schmitz-Antoniak, Detlef Schmitz, Anne Warland, Masih Darbandi, Soumyajyoti Haldar, Sumanta Bhandary, Biplab Sanyal, Olle Eriksson, and Heiko Wende*

The Verwey transition in Fe_3O_4 nanoparticles with a mean diameter of 6.3 nm is suppressed after capping the particles with a 3.5 nm thick shell of SiO_2. By X-ray absorption spectroscopy and its associated X-ray magnetic circular dichroism this suppression can be correlated to localized Fe^{2+} states and a reduced double exchange visible in different site-specific magnetization behavior in high magnetic fields. The results are discussed in terms of charge trapping at defects in the Fe_3O_4/ SiO_2 interface and the consequent difficulties in the formation of the common phases of Fe_3O_4. By comparison to X-ray absorption spectra of bare Fe_3O_4 nanoparticles in course of the Verwey transition, particular changes in the spectral shape could be correlated to changes in the number of unoccupied d states for Fe ions at different lattice sites. These findings are supported by density functional theory calculations.

1. Introduction

Magnetite (Fe_3O_4) nanoparticles are the subject of intense research activities driven both by basic research and their possible use in various applications. They can be used e.g. as contrast agents in magnetic resonance imaging[1–3] for hyperthermia cancer treatment, targeted drug delivery, rotary shaft sealing, oscillation damping, position sensing,[4] magnetic inks for jet printing,[5] and to remove heavy metals from wastewater.[6,7] In addition, due to the half-metallicity with a predicted negative spin polarization[8,9] in its cubic phase, magnetite is an interesting candidate for spintronics[10] at room temperature and above.

Magnetite is the Fe oxide with the highest net magnetic moment and crystallizes in a cubic inverse spinel structure. In a simple picture, it consists of Fe^{2+} ions on octahedral (O_h) lattice sites, Fe^{3+} on octahedral and Fe^{3+} on tetrahedral (T_d) lattice sites. Although it is well known that due to hybridization effects the charges of the ions differ from the nominal values, we will use this notation here to distinguish between the different Fe species and denote them $Fe^{2+}{}_{Oh}$, $Fe^{3+}{}_{Oh}$, and $Fe^{3+}{}_{Td}$, respectively.

Below its Curie temperature of about 860 K, magnetite is a ferrimagnet due to an oxygen-mediated antiferromagnetic 125° superexchange between Fe ions on O_h and T_d sites. A ferromagnetic order between Fe ions on the O_h sites is a consequence of superexchange, double exchange (between $Fe^{2+}{}_{Oh}$, and $Fe^{3+}{}_{Oh}$ ions), and direct exchange. At a temperature of about 123 K magnetite undergoes a phase transition, the so-called Verwey transition[11] accompanied by a spin re-orientation transition at slightly higher temperature[12] characterized by vanishing magnetocrystalline anisotropy. In the low temperature phase, magnetite has a monoclinic structure and exhibits

Dr. C. Schmitz-Antoniak
Peter-Grünberg-Institut (PGI-6)
Forschungszentrum Jülich
52425 Jülich, Germany
E-mail: c.schmitz-antoniak@fz-juelich.de
Dr. D. Schmitz
Helmholtz-Zentrum Berlin für Materialien und Energie
Albert-Einstein-Str.15, 12489 Berlin, Germany
Dr. A. Warland, Dr. M. Darbandi, Prof. H. Wende
Fakultät für Physik and Center for Nanointegration Duisburg-Essen (CENIDE)
Universität Duisburg-Essen
Lotharstr. 1, 47048 Duisburg, Germany
Dr. M. Darbandi
Chemistry faculty
University of Tabriz
Tabriz, Iran
Dr. S. Haldar
Institute of Theoretical Physics & Astrophysics
University of Kiel
Leibnizstr. 15, 24098 Kiel, Germany
Dr. S. Bhandary
Centre de Physique Théorique (CPHT)
Ecole Polytechnique
91128 Palaiseau cedex, France
Dr. B. Sanyal, Prof. O. Eriksson
Division of Materials Theory
Department of Physics and Astronomy
Uppsala University
Box-516, SE, 75120 Uppsala, Sweden
Prof. O. Eriksson
School of Science and Technology
Örebro University
SE 70182 Örebro, Sweden
The ORCID identification number(s) for the author(s) of this article can be found under https://doi.org/10.1002/andp.201700363

DOI: 10.1002/andp.201700363

charge ordering[13,14] and orbital ordering on the Fe^{2+} sites.[15,16] In addition it was found that localized electrons are shared between three Fe ions on O_h sites which can be viewed as quasiparticles and were named trimerons.[17] In agreement to this model, a reduction of the exchange interaction between Fe ions on O_h lattice sites was reported.[18] In the Supporting Information we present how this weakened double exchange below the Verwey transition temperature influences the site-specific spin canting in a 200 nm thick reference film.

In ensembles of nanoparticles, the Verwey transition is difficult to be observed by diffraction methods, magnetometry or resistivity measurements as already discussed elsewhere.[19] While tunnel spectroscopy[20] and scanning tunneling microspectroscopy[21,22] have been used to investigate the Verwey transition in single nanoparticles, analysis of the X-ray absorption near-edge structure (XANES) and its associated magnetic circular dichroism (XMCD) has turned out to be a powerful tool to monitor the transition in ensembles of magnetite nanoparticles.[23] Hence it is used in this work to investigate the influence of a 3.5 nm thick amorphous silica (SiO_2) shell on the properties of magnetite nanoparticles with a mean diameter of (6.3 ± 0.9) nm. In particular, we focus on the influence on the Verwey transition, spin canting effects and (temperature-dependent) changes of the XANES that reflects the unoccupied 3d density of states. The results are discussed regarding charge trapping at the magnetite/silica interface and related reduced double exchange.

2. Results

Temperature-dependent XANES and XMCD measurements are shown in **Figure 1** for bare magnetite nanoparticles (upper panel) and silica capped magnetite nanoparticles (lower panel). For a discussion of the fine structure the spectra are shown in a reduced energy range around the two absorption edges. Spectra taken in the low temperature regime (4 K, 50 K) are plotted as blue lines, spectra of the high-temperature phase (100 K, 115 K, 130 K, 150 K) in red. The violet colored line corresponds to an intermediate temperature of 75 K. Before turning to the temperature-dependent changes of XANES and XMCD, the main spectral features will be compared. At the L_3 absorption edge, the XANES shows two small peaks in the pre-edge region denoted A and B that can be assigned to contributions of $Fe^{2+}{}_{Oh}$. These peaks are more pronounced and sharper for the silica capped magnetite nanoparticles compared to the bare ones indicating a higher fraction of $Fe^{2+}{}_{Oh}$ ions and a stronger localization of the 3d states, respectively. These ions are also mainly responsible for the first main peak (C) in the XANES spectra together with small contribution of $Fe^{3+}{}_{Oh}$. The second main peak (D) comes from $Fe^{3+}{}_{Oh}$ and $Fe^{3+}{}_{Td}$ ions. From the ratio of the amplitudes of peak C to D, the fraction of $Fe^{2+}{}_{Oh}$ can be estimated. Since peak C is smaller in comparison to peak D for the case of bare magnetite nanoparticles, one can conclude that these nanoparticles are oxidized towards γ-Fe_2O_3 whereas the silica shell prevents the nanoparticles from further oxidation in agreement to previously published results.[24]

At the L_2 absorption edge, the first peak (E) originates again from $Fe^{2+}{}_{Oh}$, while the two other peaks (F and G) can be assigned to Fe^{3+} ions with an additional contribution from Fe^{2+} ions. Again, the amplitude of peak E and the ratio of peaks F to G can be used for a rough estimation of the quality of magnetite. Particularly, peak F is higher than peak G for magnetite. By comparison with reference data of non-stoichiometric $Fe_{3-\delta}O_4$ epitaxial films,[25] one can estimate $0.13 < \delta < 0.23$ for our bare magnetite nanoparticles and $\delta \approx 0$ for the silica capped ones.

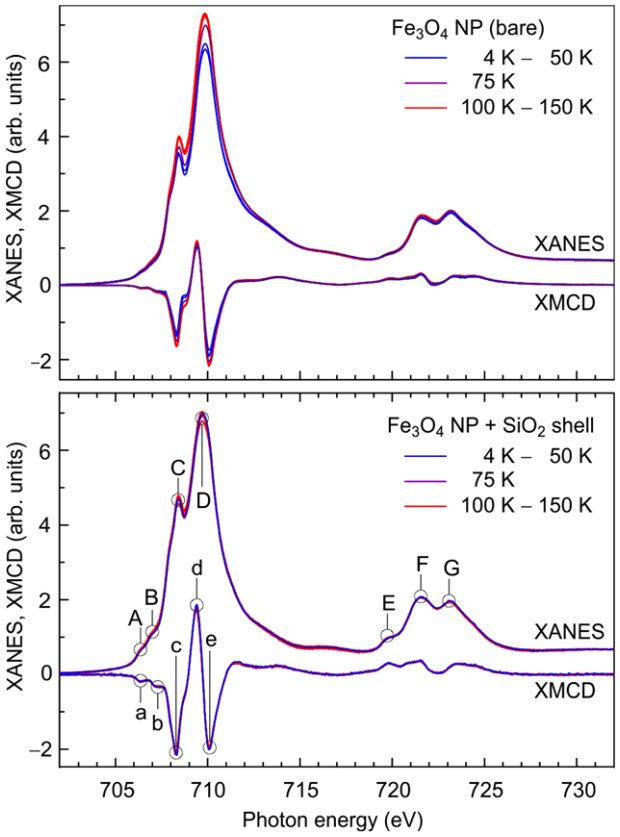

Figure 1. X-ray absorption near-edge structure (XANES) and X-ray magnetic circular dichroism (XMCD) for bare magnetite nanoparticles (upper panel) and silica capped magnetite nanoparticles (lower panel) at various temperatures. Blue lines refer to low temperatures, red lines to high temperatures, and the violet line refers to an intermediate temperature of 75 K.

The fine structure in the XMCD signal can be correlated to the different Fe species in magnetite in a similar manner. Again, the two small peaks (a and b) in the pre-edge region are caused by contributions from $Fe^{2+}{}_{Oh}$. Peak c mainly originated from $Fe^{2+}{}_{Oh}$ as well together with a small contribution from $Fe^{3+}{}_{Oh}$. The two other XMCD peaks (d and e) cannot be assigned to one single Fe ion species in a straight-forward way. The positive values of the XMCD are mainly caused by the antiferromagnetically aligned $Fe^{3+}{}_{Td}$. However, their contribution is energetically not well separated from the XMCD of $Fe^{3+}{}_{Oh}$. In a simplified picture, peak d is usually assigned to $Fe^{3+}{}_{Td}$ ions and peak e to $Fe^{3+}{}_{Oh}$ ions in magnetite. But one should keep in mind, that all Fe ions contribute to the XMCD signal in that energy region.

Having a look at the temperature dependence of XANES and XMCD, it is obvious that there is a change of the intensities between 50 K and 100 K for the bare magnetite nanoparticles (Figure 1, upper panel). These changes clearly indicate the

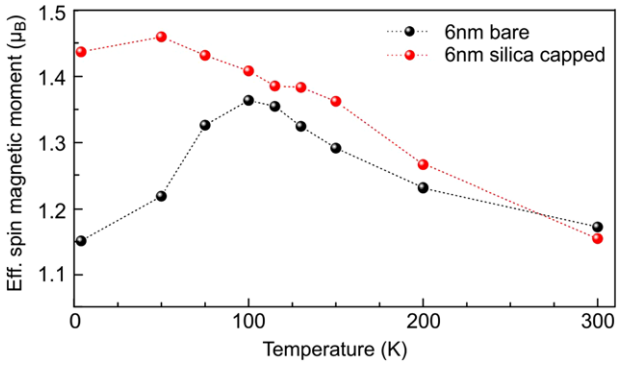

Figure 2. Temperature dependent effective spin magnetic moments at the Fe sites of bare magnetite nanoparticles (black symbols) and silica capped magnetite nanoparticles (red symbols) determined from XMCD. For all values, the total uncertainty is about 20%.

presence of the Verwey transition as discussed in the literature.[19,23] The transition is not visible in the spectra of the silica capped nanoparticles (Figure 1, lower panel). A sum rule-based analysis of the experimental data yields small average orbital magnetic moments for both samples that remain unchanged within experimental uncertainties. The temperature-dependent effective spin magnetic moment is shown in **Figure 2**. For the bare magnetite nanoparticles, a significant change in the effective spin magnetic moment marks the phase transition of magnetite.[23] For the silica capped nanoparticles, the temperature-dependent effective spin magnetic moment follows a usual M vs T behavior of a ferro- or ferrimagnet without a clear indication of the phase transition.

To measure the field-dependent magnetization of the Fe ions site-specifically, the XMCD asymmetry at three different photon energies was carefully analyzed for measurements in different magnetic fields. The first distinct minimum of the XMCD spectrum at a photon energy of $E \approx 708.3$ eV (denoted c in Figure 1) is dominated by the magnetic signal from $Fe^{2+}{}_{Oh}$ ions. Magnetization of $Fe^{3+}{}_{Oh}$ was determined by the XMCD asymmetry of the second distinct minimum at $E \approx 710.1$ eV (denoted e in Figure 1), and the $Fe^{3+}{}_{Td}$ mainly contribute to the maximum of the XMCD asymmetry at E ≈ 709.4 eV (denoted d in Figure 1). Note that at these energies, there is a (small) additional contribution to the XMCD signal from the other Fe ions. To analyze the spin canting, the site-specific magnetization was fitted to a power law

$$m/m_{Sat} = 1 - b\,H^n \quad (1)$$

The exponent was fixed to $n = -0.5$ as it is expected for a competition between exchange and Zeeman energies.[26,27] The fitting parameter b is a measure for the difficulty to saturate the sample magnetically. The experimental data and best fits are shown in **Figure 3**. The extracted values for the parameter b are summarized in **Table 1**. The normalized site-specific magnetization values in a magnetic field of 5 T are presented in **Table 2**. For the bare magnetite nanoparticles, the parameter b is approximately the same for all Fe ions. Its sizeable value in high magnetic fields clearly indicates spin canting effects. For silica capped magnetite nanoparticles, we find a significant reduction of the canting parameter. Particularly for the case of $Fe^{2+}{}_{Oh}$ ions, it is close to zero.

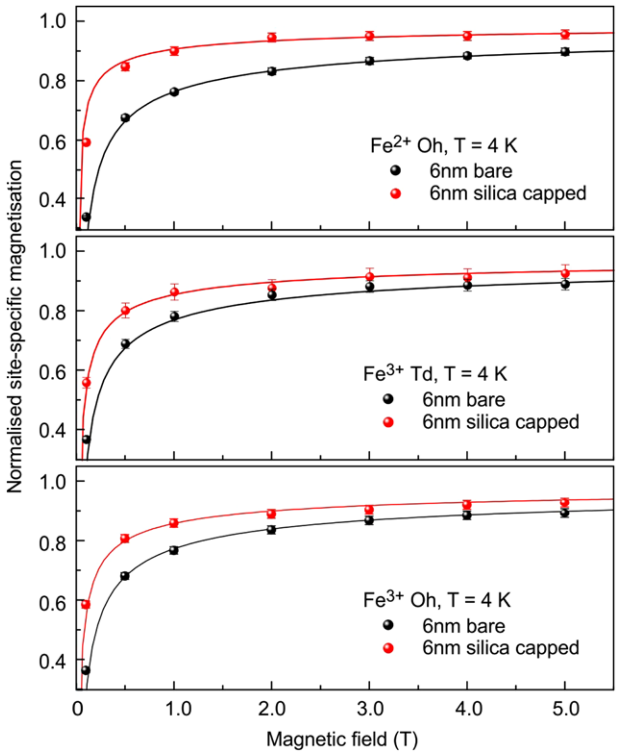

Figure 3. Normalized site-specific magnetization determined from XMCD for bare magnetite nanoparticles (black symbols) and silica capped magnetite nanoparticles (red symbols) measured at 4 K. Solid lines show fits to the experimental data.

Table 1. Site-specific canting parameter b in $T^{0.5}$ of the normalized magnetic-field-dependent XMCD asymmetry for bare and silica capped magnetite nanoparticles at $T = 4$ K.

	$b(Fe^{2+}{}_{Oh})$ [$T^{0.5}$]	$b(Fe^{3+}{}_{Td})$ [$T^{0.5}$]	$b(Fe^{3+}{}_{Oh})$ [$T^{0.5}$]
Bare	0.25 ± 0.01	0.23 ± 0.01	0.23 ± 0.01
SiO_2 capped	0.09 ± 0.01	0.14 ± 0.02	0.14 ± 0.02

Table 2. Site-specific magnetization in a magnetic field of 5 T normalized to the saturation value as obtained by fitting experimental data for bare and silica capped magnetite nanoparticles at $T = 4$ K.

	$m/m_{sat}(Fe^{2+}{}_{Oh})$	$m/m_{sat}(Fe^{3+}{}_{Td})$	$m/m_{sat}(Fe^{3+}{}_{Oh})$
Bare	(88 ± 1) %	(90 ± 2) %	(90 ± 1) %
SiO_2 capped	(96 ± 1) %	(94 ± 2) %	(94 ± 1) %

This corresponds to a magnetization in 5 T close (96%) to the saturation value while for the bare nanoparticles at these sites only 88% of the saturation magnetization could be reached.

3. Discussion

The discussion of the experimental results is split into three parts. According to the two main observations, we discuss (i) changes in the spin canting behavior of the silica capped

magnetite nanoparticles compared to the bare ones and (ii) the suppression of the Verwey transition. In addition, the suppression of the Verwey transition in silica capped nanoparticles was used to (iii) analyze changes in the electronic structure related to the Verwey transition in the uncapped species.

3.1. Site-Specific Spin Canting

In order to discuss spin canting by analysis of the magnetic-field-dependent site-specific magnetization of Fe ions, we used eq. (1) with an exponent $n = -0.5$. This equation was derived by Dieny et al.[26] for an artificial ferrimagnet and has been adopted to describe the ferrimagnetism of magnetite.[27,28] Although in the low-field region there is an influence of magnetic hysteresis and shape anisotropy originating from the magnetic dipole interaction between the nanoparticles, the experimental data can be fitted in the entire range between 0.1 T and 5 T. The bare magnetite nanoparticles exhibit a sizeable spin canting that is reflected by a large parameter b. The magnetization in an external magnetic field of 5 T is only about 88–90% for all Fe ions. The canting is slightly stronger for the $Fe^{2+}{}_{Oh}$ ions in good agreement to results obtained by Mössbauer spectroscopy.[29] The silica capped magnetite nanoparticles can be easier magnetically saturated. The magnetization in an external magnetic field of 5 T is already 94–96%. Interestingly, the spin canting is much smaller (close to zero) for the $Fe^{2+}{}_{Oh}$ ions compared to the other Fe ions. The significantly different canting behavior in silica capped magnetite nanoparticles clearly indicates that the double exchange coupling is weakened, since a strong double exchange would prevent the different canting of $Fe^{2+}{}_{Oh}$ and $Fe^{3+}{}_{Oh}$ found here. This weakening can be explained by a localization of the additional electron of $Fe^{2+}{}_{Oh}$ that mediates the double exchange in a simple picture and was discussed by McQueeney et al.[18]. For bulk material, this behavior is also found below the Verwey temperature (see Supporting Information).

In our work, this localization is visible in the sharp peaks of the XANES (XMCD) for the silica capped nanoparticles denoted A and B (a and b) in Figure 1 that do not change with temperature. The localization is related to trapped charges by defects at the magnetite/silica interface. It is well-known that defects in silica can trap both holes and electrons. For instance, capture and emission of carriers by defects in silica and silicon/silica interfaces is thought to be responsible for the 1/f noise in metal-oxide-semiconductor devices, negative bias temperature instability, and dielectric reliability and degradation.[30] The formation of stable electron trapping defects was confirmed experimentally[31,32] and by theoretical studies.[33,34] Trapped carriers were also found in larger magnetite ellipsoid-like particles (100–240 nm) capped by 3–4 nm silica[35] and attributed to localized defect states of high density in the interface region or intergranular boundaries facilitated by the large lattice mismatch between magnetite and silica.

In addition, the analysis of the site-specific canting shows that one should be careful when estimating the degree of oxidation in non-stoichiometric $Fe_{3-\delta}O_4$ by comparison with XMCD data in the literature. For the case of the bare magnetite nanoparticles, the stronger spin canting at the $Fe^{2+}{}_{Oh}$ sites yield an overestimation of the oxidation δ, while for the silica capped magnetite it leads to an underestimation. To avoid this problem, a comparison of the spectral shape of the white line is preferred.

3.2. Suppression of the Verwey Transition

The change in the effective spin magnetic moment around the transition temperature determined from XANES and XMCD spectra of bare magnetite nanoparticles is caused by a sizeable contribution of the intra-atomic spin dipole term in the low temperature phase of magnetite.[23] It is obvious from Figure 1 that the Verwey transition is suppressed in the case of the silica capped nanoparticles. In addition, Figure 2 shows that the effective spin magnetic moment is higher for the silica capped nanoparticles even at temperatures above the phase transition temperature. Since in the cubic spinel phase of the bare nanoparticles the intra-atomic spin dipole term is negligible, this difference reflects different spin magnetic moments. A reason for the reduced spin magnetic moment of the bare magnetite nanoparticles may be a slight oxidation towards a γ-Fe_2O_3-like oxide at the surface which reduces the net magnetic moment. This is supported by a different spectral shape of XANES of the bare nanoparticles compared to the ones of the capped nanoparticles as already mentioned before.

At 300 K, the effective spin magnetic moment is slightly smaller for the silica capped nanoparticles. This may indicate a reduced Curie temperature in agreement to a reduced double-exchange coupling between the different Fe ions on octahedral lattice sites that makes the different spin canting behavior possible. However, the difference in the effective spin magnetic moments are quite small and the total uncertainty is about 20%. For technical limits, it was not possible to measure at higher temperatures close to the Curie temperature in order to prove this interpretation.

The driving mechanism behind the Verwey transition is not well understood to date. It is connected to a change in both the crystallographic and electronic structure. A change in the magnetic properties can be understood as a consequence of crystallographic and electronic modifications. Assuming the crystallographic change as a driving force, one may conclude that the silica shell hampers the formation of a different crystal structure in the magnetite core. However, the crystallographic changes connected to the Verwey transition are very small[19] and silica is quite a flexible material[36] so that this explanation seems to be unlikely. In addition, no measurable influence of the silica shell on the crystal structure of magnetite was found by X-ray diffraction as presented in the Supporting Information. Despite this, a small contribution due to strain effects evolving at low temperatures cannot be excluded completely. As evident effect remains the influence of silica on the electronic properties: In agreement to the conclusion deduced from spin canting effects, trapped electrons impede the formation of the metallic high-temperature phase of magnetite. In this respect, the silica capped nanoparticles are trapped in a phase that has similar electronic properties as the low-temperature phase of magnetite. In other words, although the silica capped magnetite nanoparticles are free to change their crystallographic structure, the Verwey transition does not take place because of the modified electronic structure at the silica/magnetite interface.

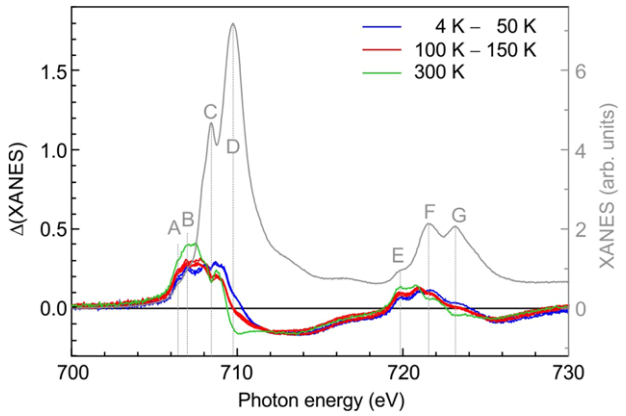

Figure 4. Relative differences of XANES of silica capped magnetite nanoparticles with respect to bare magnetite nanoparticles at different temperatures below the transition (blue lines), slightly above the transition (red lines) and well above the transition at 300 K (green line). To relate the particular changes of the spectral features of the XANES, a spectrum was added (grey line, referring to the grey scale at the right-hand side).

The Verwey transition can also be suppressed for magnetite nanoparticles covered by ligands as it is widely done to disperse the particles in a solvent. A charge transfer from Fe towards the ligand is expected to have the same effects, namely (i) reduced spin canting, particularly at the $Fe^{2+}{}_{Oh}$, (ii) reduced double exchange coupling, and (iii) a suppression of the Verwey transition. The former was already found e.g. for magnetite nanoparticles capped by oleic acid.[37]

3.3. Changes of the Electronic Structure in Course of the Verwey Transition

The suppression of the Verwey transition in silica capped nanoparticles gives the possibility to study the changes of the electronic structure in uncapped nanoparticles due to the transition in more detail. In **Figure 4** we present the relative change in the XANES of the silica capped nanoparticles with respect to the bare nanoparticles for several temperatures. The relative changes were calculated from the ratio between the normalized XANES intensity of the silica capped nanoparticles and the normalized XANES intensity of the bare nanoparticles as shown in Figure 1. An additional offset of +1 avoids division by zero in the pre-edge energy region:

$$\Delta(\mathrm{XANES}) = \frac{I_{\mathrm{XANES}}^{\mathrm{capped}} + 1}{I_{\mathrm{XANES}}^{\mathrm{bare}} + 1} - 1 \qquad (2)$$

This analysis is advantageous over a simple comparison of the XANES of bare magnetite in the low-temperature phase with the XANES in the high-temperature phase because it minimizes the influence of thermal electronic excitations to the XANES at different temperatures. Otherwise, it would be impossible to extract the transition related changes in the electronic structure from experimental data in a straightforward way.

At temperatures below the transition (blue lines), one can clearly see that the silica capped magnetite nanoparticles contain a higher fraction of $Fe^{2+}{}_{Oh}$ from the positive sign of the difference in the low energy regime of L_3 and L_2 absorption edges, where mainly $Fe^{2+}{}_{Oh}$ contribute (spectral features A, B, C at L_3 edge and E at L_2 edge). At higher energies, the difference is negative corresponding to less Fe^{3+} ions for the capped nanoparticles.

Interestingly, the transition can also be monitored in the difference Δ(XANES). This can now be used to examine the changes in the electronic configuration due to the transition in more detail. Above the transition temperature (red lines in Figure 4), the difference Δ(XANES) is even larger in the energy range that is unambiguously connected to Fe^{2+} ions (spectral features A and B) at the expense of intensity at higher energies. This is related to a small shift of XANES intensity for the bare magnetite nanoparticles towards slightly higher energies in this energy range. However, this shift is so small, that it cannot be seen directly in the XANES spectra presented in Figure 1, but it is emphasized in the plot of Δ(XANES). In a simple picture, this shift of contributions to the XANES intensity can be explained by a larger number of unoccupied d states for the $Fe^{2+}{}_{Oh}$ ions states above the transition. If we stick to the oversimplified model of 2+ and 3+ valences of Fe ions at octahedral lattice for explanation purposes, the shift will be related to a change from $Fe^{2+}{}_{Oh}$ and $Fe^{3+}{}_{Oh}$ sites in the low temperature phase to $Fe^{2.2+}{}_{Oh}$ and $Fe^{2.8+}{}_{Oh}$ in the high temperature phase. At temperatures well above the transition temperature (here: 300 K), this spectral change is very pronounced and may indicate that the transition in the bare nanoparticles takes place in a large temperature range. This reduction of the number of unoccupied d states for the Fe^{3+} ions is visible as well in the energy range well above spectral feature D at the L_3 absorption edge and well above feature G at the L_2 absorption edge related to $Fe^{3+}{}_{Oh}$ ions. However, this effect seems to be smaller and is not clearly visible due to a larger lifetime broadening of the experimental spectra.

This finding is in qualitative agreement to band structure calculations for bulk magnetite as presented in **Table 3** for the low temperature (monoclinic) phase and the high temperature (cubic) phase. The calculated number of unoccupied d states increases by about 1.3% for $Fe^{2+}{}_{Oh}$, while it remains largely constant for $Fe^{3+}{}_{Td}$ and only slightly decreases for $Fe^{3+}{}_{Oh}$. Interestingly, the changes in the experimental data correspond to larger changes in the occupation of 3d in the order of 10% rather than 1%. A possible reason is the influence of the surface that has not been taken into account in the calculation, but may play an important role. A similar underestimation of the changes in course of the Verwey transition by density functional theory were found for the change of the intra-atomic spin dipole term in magnetite nanoparticles.[23]

Table 3. Calculated site-specific number of unoccupied d states in the monoclinic (low temperature) and cubic (high temperature) phase of bulk magnetite and the relative change with increasing temperature.

	$n_h{}^{3d}(Fe^{2+}{}_{Oh})$	$n_h{}^{3d}(Fe^{3+}{}_{Td})$	$n_h{}^{3d}(Fe^{3+}{}_{Oh})$
Monoclinic[a)]	3.908	4.092	4.167
Cubic	3.962	4.096	4.147
Relat. difference	+1.3%	+0.09%	–0.16%

a) For detailed numbers of Fe ions on non-equivalent sites, see ref. [23].

The interpretation of a suppression of the Verwey transition by modifications of the electronic structure is in line with the recently published findings that electronic changes may occur at different temperatures than the structural phase transition which was found for magnetite[23] and for vanadium oxide, VO_2.[38] In the latter publication, a new monoclinic metallic phase was observed, which may be stabilized by charge doping, similar to our result.

4. Conclusion

By XANES and XMCD analyses we found that the spin canting is different for different Fe ions in magnetite nanoparticles. Particularly the spin canting of $Fe^{2+}{}_{Oh}$ ions is very sensitive to surface modifications like capping with silica. As supported by the changes in the XANES of bare magnetite nanoparticles in course of the Verwey transition and density functional theory, these ions play also a key role for the Verwey transition which is shown to be suppressed by silica capping. These observations are explained by charge-trapping at defects at the magnetite/silica interface which leads to a reduced double exchange coupling and impedes the formation of the common phases of magnetite demonstrating the important role of the electronic structure for the Verwey transition.

Experimental Section

Nanoparticle Synthesis and Sample Preparation: Magnetite nanoparticles with a narrow size distribution were synthesized using a water-in-oil microemulsion technique using Igepal CO-520 (polyoxyethylene nonylphenyl ether) as surfactant.[29] Ferrous chloride ($FeCl_2$) and ferric chloride ($FeCl_3$) were used as precursors for Fe^{2+} and Fe^{3+} respectively. By hydrolysis of TEOS (tetraethylorthosilicate), the magnetite nanoparticles were coated with a silica shell in a second step. For both bare and silica coated magnetite nanoparticles, the surfactants were removed by several washing steps with butanol, propanol, and ethanol. The nanoparticles were collected subsequently by centrifugation and redispersed in ethanol. The size distribution and shell thickness are determined by transmission electron microscopy images. The magnetite nanoparticles have a mean diameter of (6.3 ± 0.9) nm and the silica shell has a thickness of about 3.5 nm as published before.[24] By Mössbauer spectroscopy we could prove that there is no relevant cation disorder.[29] For our experimental work presented here, the nanoparticles were brought onto a naturally oxidized p-doped Si wafer by drop coating. In order to minimize oxidation of the bare Fe_3O_4 nanoparticles, the particles were freshly prepared and quickly inserted into the load lock of the UHV system after the coating procedure. However, the formation of a thin γ-Fe_2O_3-like surface layer cannot be avoided.

X-ray Absorption Spectroscopy: XANES and XMCD measurements were carried out at the high-field end station of the variable polarization beamline UE46-PGM1 at the HZB - BESSY II synchrotron radiation facility in Berlin. Fe spectra were taken at the $L_{3,2}$ absorption edges (probing the spin-orbit split $2p_{3/2} \rightarrow 3d$ and $2p_{1/2} \rightarrow 3d$ electron transitions) in the photon energy range of 680 eV $\leq E \leq$ 780 eV. All spectra were taken in normal X-ray incidence with the magnetic field parallel or antiparallel to the wave vector of incoming X-rays. The absorption was detected in total electron yield mode by measuring the sample drain current. For temperature-dependent measurements, the sample was cooled down to $T = 4$ K in an applied magnetic field of -0.5 T. The XMCD was measured at several temperatures in an applied magnetic field of $+3$ T which was kept constant during heating. The two samples – bare and silica capped magnetite nanoparticles – were mounted on the same sample holder and measured in quick succession at each stabilized temperature to ensure an identical sample history and treatment.

Magnetic-field-dependent measurements were carried out at $T = 4$ K from $+5$ T to 0 T and from -5 T to 0 T. To obtain site-specific magnetization curves we measured full spectra at various magnetic fields.

Density Functional Theory: Site-specific d charges (and magnetic moments as presented elsewhere[23]) in magnetite were calculated using the projector augmented wave method[39,40] as implemented in plane-wave based density functional code VASP[41] within the generalized gradient approximation (GGA) as given by Perdew, Burke and Ernzerhof.[42]

For all Fe 3d orbitals the exchange parameter $J = 0.89$ eV[43] was used and the on-site Coulomb interaction was included by the parameter $U = 4.5$ eV[44] to account for the strong electron correlations.

The plane wave cut-off energy was set to 400 eV. $12 \times 12 \times 12$ and $12 \times 12 \times 4$ Monkhorst–Pack k-point grids in the Brillouin zone were used for cubic and monoclinic structure, respectively. The geometries were optimized until the force on all each atom was reduced to 0.1 eV/nm.

Supporting Information

Supporting Information is available from the Wiley Online Library or from the author.

Acknowledgements

The authors thank the Helmholtz-Zentrum Berlin (HZB) for beamtime allocation and the HZB staff, in particular E. Schierle and E. Weschke, for kind support. This work was funded by BMBF (05 ES3XBA/5), DFG (WE 2623/3-1), and the Helmholtz Association (Young Investigator's Group Borderline Magnetism under contract no. VH-NG-1031).

Conflict of Interest

The authors declare no conflict of interest.

Keywords

magnetite, nanoparticles, Verwey transition, X-ray absorption spectroscopy

Received: September 29, 2017
Revised: December 21, 2017
Published online: February 26, 2018

[1] A. K. Gupta, M. Gupta, *Biomaterials* **2005**, *26*, 3995.
[2] S. Laurent, D. Forge, M. Port, A. Roch, C. Robic, L. Vander Elst, R. N. Muller, *Chem. Rev.* **2008**, *108*, 2064.
[3] M. Darbandi, S. Laurent, M. Busch, Z. Li, Y. Yuan, M. Krüger, M. Farle, M. Winterer, L. Elst, R. Muller, H. Wende, *J. Nanoparticle Res.* **2013**, *15*, 1664.
[4] K. Raj, R. Moskowitz, *J. Magn. Magn. Mater.* **1990**, *85*, 233.
[5] S. W. Charles, J. Popplewell, *Endeavour* **1982**, *6*, 153.
[6] L. Carlos, F. S. García Einschlag, M. C. González, D.O. Mártire in *Waste Water - Treatment Technologies and Recent Analytical Developments*, InTech, Rijeka, **2013**, p. 63.
[7] P. Xu, G. Ming Zeng, D. Lian Huang, C. Ling Feng, S. Hu, M. Hua Zhao, C. Lai, Z. Wei, C. Huang, G. Xin Xie, Z. Feng Liu, *Sci. Total Environ.* **2012**, *424*, 1.
[8] Z. Zhang, S. Satpathy, *Phys. Rev. B* **1991**, *44*, 13319.
[9] Y. S. Dedkov, U. Rüdiger, G. Güntherodt, *Phys. Rev. B* **2002**, *65*, 064417.
[10] S. Parkin, X. Jiang, C. Kaiser, C. Panchula, K. Roche, M. Samant, *Proc. IEEE* **2003**, *91*, 661.
[11] E. J. W. Verwey, *Nature* **1939**, *144*, 327.
[12] Ö. Özdemir, D. J. Dunlop, *Earth Planetary Sci. Lett.* **1999**, *165*, 229239.
[13] J. P. Wright, J. P. Attfield, P. G. Radaelli, *Phys. Rev. Lett.* **2001**, *87*, 266401.
[14] J. P. Wright, J. P. Attfield, P. G. Radaelli, *Phys. Rev. B* **2002**, *66*, 214422.
[15] H.-T. Jeng, G. Y. Guo, D. J. Huang, *Phys. Rev. Lett.* **2004**, *93*, 156403.
[16] J. Schlappa, C. Schüßler-Langeheine, C. F. Chang, H. Ott, A. Tanaka, Z. Hu, M. W. Haverkort, E. Schierle, E. Weschke, G. Kaindl, L. H. Tjeng, *Phys. Rev. Lett.* **2008**, *100*, 026406.
[17] M. S. Senn, J. P. Wright, J. P. Attfield, *Nature* **2012**, *481*, 173.
[18] R.J. McQueeney, M. Yethiraj, S. Chang, W. Montfrooij, T. G. Perring, J. M. Honig, P. Metcalf, *Phys. Rev. Lett.* **2007**, *99*, 246401.
[19] C. Schmitz-Antoniak, D. Schmitz, A. Warland, N. Svechkina, S. Salamon, C. Piamonteze, H. Wende, *Sci. Rep.* **2016**, *6*, 20897.
[20] Q. Yu, A. Mottaghizadeh, H. Wang, C. Ulysse, A. Zimmers, V. Rebuttini, N. Pinna, H. Aubin, *Phys. Rev. B* **2014**, *90*, 075122.
[21] P. Poddar, T. Fried, G. Markovich, A. Sharoni, D. Katz, T. Wizansky, O. Millo, *Europhys. Lett.* **2003**, *64*, 98.
[22] A. Hevroni, M. Bapna, S. Piotrowski, S. A. Majetich, G. Markovich, *Phys. Chem. Lett.* **2016**, *7*, 1661.
[23] D. Schmitz, C. Schmitz-Antoniak, A. Warland, M. Darbandi, S. Haldar, S. Bhandary, O. Eriksson, B. Sanyal, H. Wende, *Sci. Rep.* **2014**, *4*, 5760.
[24] A. Warland, C. Antoniak, M. Darbandi, C. Weis, J. Landers, W. Keune, H. Wende, *Phys. Rev. B* **2012**, *85*, 235113.
[25] E. Pellegrin, M. Hagelstein, S. Doyle, H. O. Moser, J. Fuchs, D. Vollath, S. Schuppler, M. A. James, S. S. Saxena, L. Niesen, O. Rogojanu, G. A. Sawatzky, C. Ferrero, M. Borowski, O. Tjernberg, N. B. Brookes, *Phys. Status Solidi B* **1999**, *215*, 797.
[26] B. Dieny, D. Givord, J. M. B. Ndjaka, *J. Magn. Magn. Mater.* **1991**, *93*, 503.
[27] D. T. Margulies, F. T. Parker, M. L. Rudee, F. E. Spada, J. N. Chapman, P. R. Aitchison, A. E. Berkowitz, *Phys. Rev. Lett.* **1997**, *79*, 5162.
[28] J.-B. Moussy, S. Gota, A. Bataille, M.-J. Guittet, M. Gautier-Soyer, F. Delille, B. Dieny, F. Ott, T. D. Doan, P. Warwin, P. Bayle-Guillemaud, C. Gatel, E. Snoek, *Phys. Rev. B* **2004**, *70*, 174448.
[29] M. Darbandi, F. Stromberg, J. Landers, N. Reckers, B. Sanyal, W. Keune, H. Wende, *J. Phys. D: Appl. Phys.* **2012**, *45*, 195001.
[30] A. V. Kimmel, P. V. Sushko, A. L. Shluger, G. Bersuker, *ECS Trans.* **2009**, *19*, 3.
[31] M. Walters, A. Reisman, *J. Electrochem. Soc.* **1991**, *138*, 2755.
[32] V. V. Afanasev, A. Stesmans, *Phys. Rev. Lett.* **1997**, *78*, 2437.
[33] P. V. Sushko, S. Mukhopadhyay, A. M. Stoneham, A. L. Shluger, *Microelectr. Eng.* **2005**, *80*, 292.
[34] A.-M. El-Sayed, M. B. Watkins, V. V. Afanasev, A. L. Shluger, *Phys. Rev. B* **2014**, *89*, 125201.
[35] C.-C. Chang, L. Zhao, M.-K. Wu, *J. Appl. Phys.* **2010**, *108*, 094105.
[36] S. Yamamoto, K. Sonobe, T. Miyashita, M. Mitsuishi, *J. Mater. Chem. C* **2015**, *3*, 1286.
[37] A. G. Roca, D. Niznansky, J. Poltierova-Vejpravova, B. Bittova, M.A. González-Fernández, C. J. Serna, M. P. Morales, *J. Appl. Phys.* **2009**, *105*, 114309.
[38] Z. Tao, T.-R. T. Han, S. D. Mahanti, P. M. Duxbury, F. Yuan, C.-Y. Ruan, *Phys. Rev. Lett.* **2012**, *109*, 166406.
[39] P. E. Blöchl, *Phys. Rev. B* **1994**, *50*, 17953.
[40] G. Kresse, D. Joubert, *Phys. Rev. B* **1999**, *59*, 1758.
[41] G. Kresse, G. J. Furthmüller, *Phys. Rev. B* **1996**, *54*, 11169.
[42] J. P. Perdew, K. Burke, M. Ernzerhof, *Phys. Rev. Lett.* **1996**, *77*, 3865.
[43] V. I. Anisimov, J. Zaanen, O. K. Andersen, *Phys. Rev. B* **1991**, *44*, 943.
[44] V. I. Anisimov, I. S. Elfimov, N. Hamada, K. Terakura, *Phys. Rev. B* **1196**, *54*, 4387.